

---

# Closed-form Symbolic Solutions: A New Perspective on Solving Partial Differential Equations

---

Shu Wei<sup>12†\*</sup>, Yanjie Li<sup>12†</sup>, Lina Yu<sup>1</sup>, Min Wu<sup>1</sup>, Weijun Li<sup>12‡</sup>, Meilan Hao<sup>1</sup>, Wenqiang Li<sup>12</sup>,  
Jingyi Liu<sup>12</sup>, Yusong Deng<sup>12</sup>

AnnLab, Institute of Semiconductors, Chinese Academy of Sciences  
Haidian, Beijing, 100083, CN  
University of Chinese Academy of Sciences  
Huairou, Beijing, 101408, CN  
weishu22@mailsucas.ac.cn

## Abstract

Solving partial differential equations (PDEs) in Euclidean space with closed-form symbolic solutions has long been a dream for mathematicians. Inspired by deep learning, Physics-Informed Neural Networks (PINNs) have shown great promise in numerically solving PDEs. However, since PINNs essentially approximate solutions within the continuous function space, their numerical solutions fall short in both precision and interpretability compared to symbolic solutions. This paper proposes a novel framework: a closed-form **S**ymbolic framework for **P**DEs (SymPDE), exploring the use of deep reinforcement learning to directly obtain symbolic solutions for PDEs. SymPDE alleviates the challenges PINNs face in fitting high-frequency and steeply changing functions. To our knowledge, no prior work has implemented this approach. Experiments on solving the Poisson's equation and heat equation in time-independent and spatiotemporal dynamical systems respectively demonstrate that SymPDE can provide accurate closed-form symbolic solutions for various types of PDEs.

## 1 Introduction

Partial differential equations (PDEs) widely exist in the fields of mathematics, physics and other natural sciences. They are the product of abstract modeling of natural physical phenomena. For example, the Poisson equation can be used to describe the distribution of electrostatic potential, and the heat equation can be used to describe changes in the temperature of an object. etc[1]. Understanding and predicting the dynamics of complex physical systems necessitates the resolution of these PDEs—an endeavor that has captivated mathematicians for several centuries.

Achieving analytical solutions to the systems' PDEs involves rigorous examination of the solutions' existence, uniqueness, and stability, as well as their behavioral characteristics, entailing multifaceted mathematical theories and computational techniques. For example, constructing analytical solutions to linear PDEs via the superposition principle requires first determining the Green's functions  $G(\mathbf{x}, \mathbf{x}')$  [2]—a fundamental solution to a PDE with a point source located at  $\mathbf{x}'$ —and then convolving this function with the source term, which demands profound insights into the properties of Green's functions, particularly under complex boundary conditions or multidimensional spaces. In the context of nonlinear PDEs, due to their inherent nonlinearity, obtaining analytic solutions is exceedingly

---

\*This work was supported in part by the National Natural Science Foundation of China under Grant 92370117, in part by CAS Project for Young Scientists in Basic Research under Grant YSBR-090.

†Equal Contribution.

‡Corresponding Author.

challenging, frequently mandating recourse to numerical methods; however, accurately solving certain nonlinear PDEs, such as the Navier-Stokes equations, incurs prohibitively high computational costs. Methods from the realm of deep learning introduce a data-driven approach for the numerical resolution of PDEs.

The Physics-Informed Neural Networks (PINNs) methodology[3], leveraging the universal approximation theorem[4], has showcased its effectiveness in approximating solution functions across various PDE systems. However, the full connected neural networks(FCNNs) used in dominant physics-informed learning model, the PINN[5], often demonstrate limited proficiency in approximating high-frequency and steep functions, leading to significant discrepancies in numerical solutions within oscillatory or distorted regions[6]. The introduction of neural operator methods, such as Deep Operator Network (DeepONet)[7] and the Fourier Neural Operator(FNO)[8], which learn mappings between functions, holds promise for addressing these challenges. Nevertheless, these approaches require extensive labeled data for training. Furthermore, neural network-based solutions, often perceived as black-box models, face interpretability challenges regarding the physical and mathematical characteristics of their solutions, posing difficulties when extrapolating beyond the trained domain, thereby constraining their application in scientific research.

In stark contrast, symbolic solutions inherently possess the capacity to describe complex regions, such as oscillations or distortions. For instance,  $u = |x|$  can depict the distortion of  $u$  at the origin, while  $u = \sin(5x)$  can represent a high-frequency oscillatory function. Importantly, if a symbolic solution satisfies the definitions of a PDE with closed-form inside the computational domain, it can be extrapolated to any region governed by the same PDE, demonstrating its extrapolative potential. Moreover, closed-form symbolic solutions explicitly elucidate the relationships between the solution and the variables, which is of paramount importance for the interpretation and analysis of physical problems.

Thus, we propose a method based on deep reinforcement learning to deduce closed-form symbolic solutions to PDEs without reliance on a priori complex mathematical theory or labeled data. Our main contributions are as follows:

- We introduce SymPDE, a paradigmic approach for solving PDEs, that discovers closed-form symbolic solutions satisfying the definitions of PDEs, circumventing the difficulties associated with neural network fitting of high-frequency or steep functions, while also providing extrapolative power and interpretability.
- SymPDE has been applied to time-independent PDEs, revealing the fundamental solution expressions for the Poisson equation.
- When deployed on spatiotemporal dynamical systems, SymPDE uncovers the symbolic skeleton form of the heat equation’s fundamental solution and accurately optimizes the coefficients of the skeleton.

## 2 Related work

**Physics-informed learning** Leveraging the nonlinear representational capabilities of neural networks, Physics-Informed Learning resolves the numerical solutions of PDEs within a computational domain by embedding the physical constraints of PDEs into the neural network framework. Emblematic of this approach is the PINN[5], which integrates physical constraints as inductive bias for network’s self-supervised training. However, this approach is limited by its reliance on soft constraints for physical constraints within the loss function, lacking the capacity for hard-coding physical priors. Additionally, the use of FCNNs for continuous representations of data across time and space results in suboptimal precision and efficiency, especially in the face of complex solutions with characteristics of high-frequency or steep change. In response, various enhancements to the PINN method have been proposed, including the utilization of different network architectures for discrete temporal representations[9], embedding hard-coded boundary conditions within the network[10], and segmenting and integrating large computational domains for flexible computation[11],etc. Contrary to the function approximation techniques employed by PINNs, operator learning methods like Lu et al. [7], Cai et al. [12], Li et al. [8, 13, 14] approximate nonlinear operators using neural networks to facilitate supervised solutions of PDE equations. However,the high cost of obtaining many labeled data in scientific problems hinders the application of such methods. Regardless of PINNs or neural operator learning algorithms, the outcomes represent approximate numerical solutions of

PDEs, lacking interpretability in relation to physical phenomena and exhibiting weak extrapolative capabilities.

**Symbolic regression** The field of symbolic regression currently encompasses a plethora of distinct algorithms that can be categorized into three principal classes. The first class encompasses algorithms based on the exploration of the solution space, including conventional genetic programming (GP)[15, 16, 17, 18, 19, 20] and heuristic search strategies. However, these traditional approaches are characteristically complex in computation and heavily dependent on hyperparameters. In response to these limitations, researchers such as Sahoo et al. [21] have incorporated neural networks to constrain the search space, culminating in a series of extended works. There have also been approaches employing reinforcement learning algorithms for symbolic regression tasks [22, 23, 24], involving strategies such as policy gradient methods and Monte Carlo tree searches [25], with subsequent endeavors integrating diverse algorithms. These methods exhibit slower inference times since they necessitate iterative searches during inference. The second category is inspired by the paradigm of large-scale supervised pre-training. Numerous studies[26, 27, 28] have employed supervised training on expansive synthetically generated datasets for the end-to-end generation of expressions, significantly expediting inference speeds. However, the efficacy of these methods is compromised under conditions where discrepancies exist between the data distribution of actual physical systems and the training set, leading to diminished model performance. Lastly, an array of methodologies adopting a hybrid of search and supervised learning has been executed to perform symbolic regression tasks, achieving commendable results[29].

**Computer algebra systems and Symbolic regression based on numerical solution of PDE** Some existing methods can also obtain symbolic solutions. For example, SymPy[30], as a Computer algebra system, has a built-in method for solving PDEs. However, the method is based on mathematical symbol deduction, which is not only slow to solve, but also can only solve the first-order partial differential equation. The potent capacity of symbolic regression for uncovering expressive formulations, coupled with its high interpretability, offers the potential for devising understandable symbolic solutions for PDEs. Podina et al. [31], Majumdar et al. [32] initially employs the PINNs methodology to ascertain numerical solutions to PDEs, subsequently invoking symbolic regression techniques to identify interpretable symbolic expressions. However, an intrinsic flaw exists in this methodology: the numerical solutions derived via deep learning techniques such as PINNs are invariably approximative. Conducting symbolic regression on such imprecise data inevitably leads to substantial deviations.

### 3 Methodology

#### 3.1 Characterizing multiple PDEs

SymPDE can solve the governing PDEs of various systems, including time-independent nonlinear systems as well as spatiotemporal dynamical systems, with closed-form symbolic solutions. This section will elucidate how the SymPDE characterizes the PDEs.

**Time-independent systems** Consider a PDE associated with an unknown multivariate function and its partial derivatives. Within an bounded domain  $\Omega \subset \mathbb{R}^{(n)}$ , let the point in  $\Omega$  be denoted by  $\mathbf{x} = (x_1, x_2, \dots, x_n)$ , and  $u(\mathbf{x})$  represents the function to be determined. For a fixed positive integer  $k$ ,  $\nabla^k u \in \mathbb{R}^{n^k}$  denotes all partial derivatives of  $u$ . Given a function  $\mathcal{F} : \mathbb{R}^{n^k} \times \mathbb{R}^{n^{k-1}} \times \dots \times \mathbb{R}^n \times \mathbb{R} \times \Omega \rightarrow \mathbb{R}$ , the form of a partial differential equation of order  $k^{th}$  can be defined as equation 1 subject to boundary conditions  $\mathcal{B}(u, \nabla_{\mathbf{x}} u, \dots; \mathbf{x} \in \partial\Omega) = 0$ . The Poisson's equation 2 is a typical equation describing the time-independent system.

$$\mathcal{F}[\mathbf{x}, u(\mathbf{x}), \nabla_{\mathbf{x}} u(\mathbf{x}), \dots, \nabla_{\mathbf{x}}^{k-1} u(\mathbf{x}), \nabla_{\mathbf{x}}^k u(\mathbf{x})] = 0 \quad (1)$$

$$-\Delta u(\mathbf{x}) = f(\mathbf{x}) \quad (2)$$

We use expression skeleton  $\hat{u}(\mathbf{x})$  to represent the solution of this system. For instance,  $\hat{u} = c_1 x_1 + c_2 \sin(x_2)$  consists of constants  $c_1, c_2$ , closed-form symbols  $\{+, \times, \sin\}$ , and variables  $x_1, x_2$ . To get the closed-form solution, we replace the constants with variable parameters to construct a computational graph based on the expression skeleton. By randomly sampling data points  $\mathbf{x}$  within

the domain  $\Omega$  as input to the computational graph, and employing automatic differentiation to compute  $\nabla_{\mathbf{x}}\hat{u}, \nabla_{\mathbf{x}}^2\hat{u}, \dots$ , we obtain the forward computation results for  $\mathcal{F}$  and the boundary conditions  $\mathcal{B}$  in the equation 1. We use nonlinear optimization algorithms such as the BFGS algorithm to optimize the constants component by minimize the sum of mean square errors  $\mathcal{L}_s$ (equation 3). Here,  $\{\mathbf{x}_f^i\}_{i=1}^{N_{\mathcal{F}}}$  denotes the collocation points on  $\mathcal{F}$ ,  $\{\mathbf{x}_b^i, u_b^i\}_{i=1}^{N_{\mathcal{B}}}$  denotes the collocation points on the boundary. The loss after we optimize the constants measures the degree of consistency between the solution and the PDE.

$$\begin{cases} \mathcal{L}_s = \overline{\text{MSE}_{\mathcal{F}} + \text{MSE}_{\mathcal{B}}} \\ \text{MSE}_{\mathcal{F}} = \frac{1}{N_{\mathcal{F}}} \sum_i^{N_{\mathcal{F}}} |\mathcal{F}(\mathbf{x}_f^i)|^2 \\ \text{MSE}_{\mathcal{B}} = \frac{1}{N_{\mathcal{B}}} \sum_i^{N_{\mathcal{B}}} |\hat{u}(\mathbf{x}_b^i) - u_b^i|^2 \end{cases} \quad (3)$$

**Continuous time model for spatiotemporal dynamical system** Many physical dynamic systems in the real world have solution functions that vary over time. These functions are often represented by partial differential equations in the equation 4's form.

$$u_t(\mathbf{x}, t) = \mathcal{N}(\mathbf{x}, t, \nabla_{\mathbf{x}}u(\mathbf{x}, t), \dots, \nabla_{\mathbf{x}}^{k-1}u(\mathbf{x}, t), \nabla_{\mathbf{x}}^k u(\mathbf{x}, t)) \quad (4)$$

$$u_t(\mathbf{x}, t) - a^2 \Delta u = f(\mathbf{x}, t), \text{ where } a > 0 \text{ and } a \text{ is a cons.} \quad (5)$$

Solution  $u(\mathbf{x}, t) \in \mathbf{R}^{(n)}$  is defined within the spatiotemporal domain  $(\mathbf{x}, t) \in \Omega \times \tau$ . A typical example is the heat equation(equation 5). Apart from boundary conditions, the solution of these problems requires the specification of initial conditions  $\mathcal{I}(u; t = 0, \mathbf{x} \in \Omega) = 0$ . For such spatiotemporal dynamical systems, we can treat the time dimension and the space dimension as equivalent to establish a continuous time model. Specifically, we must construct computational graphs based on a spatial-temporal coupled expression skeletons, for instance, of  $u = cx^2e^{-t}$ . We sample data points across the spatiotemporal domain  $\Omega \times \tau$  and compute  $(u_t - \mathcal{N}), \mathcal{B}, \mathcal{I}$  to optimize the constants by minimize  $\mathcal{L}_{s-t}$ (equation 6) as shown in figure 1. Here,  $\{\mathbf{x}_n^i, t_n^i\}_{i=1}^{N_{\mathcal{N}}}$  denotes the collocation points on  $\mathcal{N}$ ,  $\{\mathbf{x}_b^i, t_b^i, u_b^i\}_{i=1}^{N_{\mathcal{B}}}$  denotes the collocation points on the boundary,  $\{\mathbf{x}_0^i, u_0^i\}_{i=1}^{N_{\mathcal{I}}}$  denotes the initial data. The loss after we optimize the constants measures the degree of consistency between the solution and the PDE.

$$\begin{cases} \mathcal{L}_{s-t} = \overline{\text{MSE}_{\mathcal{N}} + \text{MSE}_{\mathcal{B}} + \text{MSE}_{\mathcal{I}}} \\ \text{MSE}_{\mathcal{N}} = \frac{1}{N_{\mathcal{N}}} \sum_i^{N_{\mathcal{N}}} |\hat{u}_t - \mathcal{N}(x_n^i, t_n^i)|^2 \\ \text{MSE}_{\mathcal{B}} = \frac{1}{N_{\mathcal{B}}} \sum_i^{N_{\mathcal{B}}} |\hat{u}(x_b^i, t_b^i) - u_b^i|^2 \\ \text{MSE}_{\mathcal{I}} = \frac{1}{N_{\mathcal{I}}} \sum_i^{N_{\mathcal{I}}} |\hat{u}(x_0^i, 0) - u_0^i|^2 \end{cases} \quad (6)$$

**Discrete time model for spatiotemporal dynamical system** The incorporation of temporal variables in spatiotemporal systems expands the search space for symbolic solutions, complicating the quest for complex solutions. Inspired by the Finite Difference Time Domain (FDTD) numerical method[33], we mitigate the complexity of finding closed-form solutions by introducing a discrete time model that parameterizes the time variable. Suppose that within the temporal domain  $t \in \tau$ , each moment  $t$  corresponds to the solution  $u^t$ , which can be represented by one spatial coordinate-based expression skeleton  $\hat{u}(\mathbf{x}; \vec{\alpha}_t)$  over time shown in figure 1(b). Note the constant term of solution's skeleton evolves into a time-varying parameter  $\vec{\alpha}_t$ , rendering the solution a parametric equation. In order to construct the forward calculation graph of the expression on the left side of equation 4, in time domain  $\tau$ , We first randomly collect  $N_{\mathcal{N}}$  pairs of time points with extremely small time intervals at a high frequency  $M \text{ Hz}: \{(t_i^0, t_i^1) | (t_i^1 - t_i^0) = 1/M, i = 0, 1, \dots, N_{\mathcal{N}}\}$ . We use the time difference method to calculate derivative term  $\hat{u}_{t_i^0}$ , and minimize  $\mathcal{L}_{s-t}$  based on the boundary data and initial data to optimize the constant. After determining the skeleton of the expression, to approximate the nonlinear mapping from time  $t$  to parameters  $\vec{\alpha}_t$ , we construct a fully connected neural network, called the parametric neural network (PNN), outputting  $\vec{\alpha}(t; \theta_{\text{PNN}})$  as shown in figure 1(c). In order to calculate  $\mathcal{L}_{s-t}$  accurately, we sample time points at equal intervals in the time domain with frequency  $M$  (i.e.  $N_{\mathcal{N}} = M$ ) to construct discrete convolutions over time shown in figure 1(d). and optimize  $\theta_{\text{PNN}}$  by minimizing  $\mathcal{L}_{s-t}$  with the Adam and BFGS algorithms.

### 3.2 Expression generation and optimization based on reinforcement learning

We incorporate the symbolic regression methodology proposed in Petersen et al. [22] to accomplish the generation and optimization of closed-form symbolic solutions for PDEs based on reinforcement

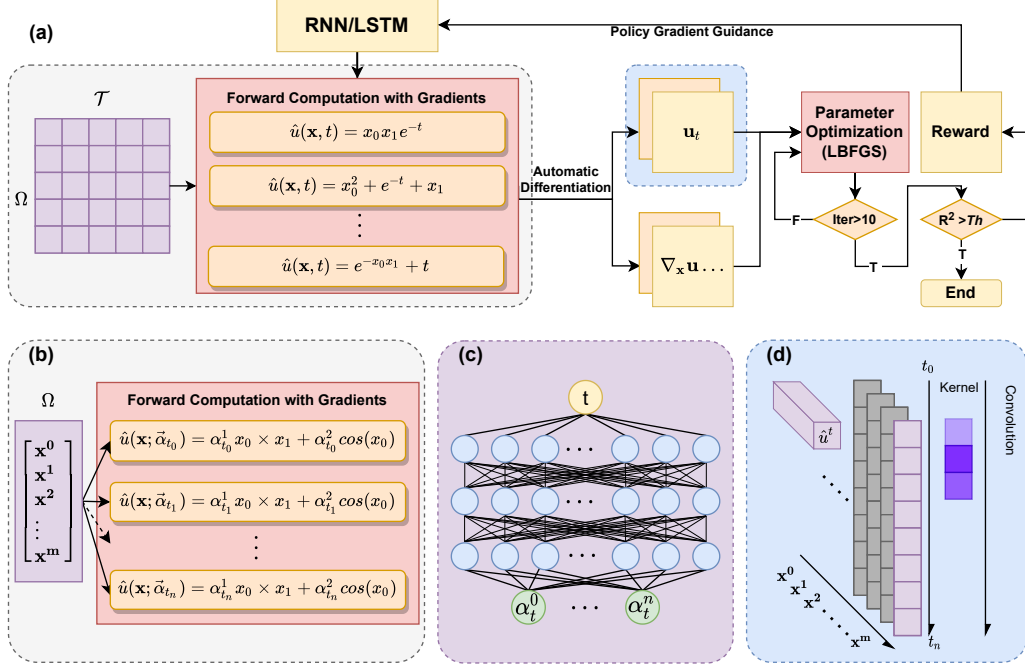


Figure 1: (a) The flowchart of SymPDE: initially, the RNN generates various expression skeletons, with space and time variables as the independent variables. The constants are optimized using the known conditions of the PDE to calculate the reward, which is used to update the RNN parameters until reward  $> 0.9999$ . (b) In time-discrete model, the RNN generates identical parametric expression skeletons, whose independent variable is the spatial variable. (c) The parameterization of expression skeleton, a Parameter Neural Network (PNN) is employed. PNN takes time  $t$  as input and outputs the parameters within the expression skeleton. (d) In discrete-time model, denote solution expressions at different moments as  $\hat{u}^t$ , and using differential convolution forms to calculate the temporal derivatives of the solution across discrete time steps.

learning. Specifically, we employ a recurrent neural network (RNN) to generate expression skeletons of solutions and optimized the constants using the techniques outlined in Section 3.1. Upon convergence, we obtain a set of compact symbolic expressions. To evaluate these expressions, we develop kinds of losses (equation 3 and 6). Since the losses are non-differentiable with respect to the parameters of the RNN,  $\theta_{\text{exp}}$ , we optimized the RNN through policy gradient methods aimed at maximizing a reward function defined by equation 7 and 8. Below, we elaborate on the process of generating and optimizing expressions, with more details available in Petersen et al. [22].

**Expressions generation** We leverage symbolic expression trees where internal nodes represent mathematical operators, and terminal nodes are input variables or constants. This representation not only accommodates unary and binary operators but also permits the sequential generation of expression trees through pre-order traversal, thus the pre-order traversal of its corresponding expression tree  $\tau$  can represent an closed-form solution  $\hat{u}$ . Building on this, we employ a RNN to generate the expression tokens in an autoregressive manner, where the probability of choosing each token  $\tau_i$  (e.g.  $+$ ,  $-$ ,  $\times$ ,  $\div$ ,  $\dots$ ) is determined by a probability vector output by RNN, processed through a softmax layer to ensure contextual dependency on previously chosen symbols. We provide the RNN with representations of the parent and sibling nodes of the token being sampled, thus reinforcing the model to understand the expression tree structure.

**Reward definition** Viewing the task of discovering closed-form solutions for PDEs as a Markov Decision Process (MDP) comprising the elements  $(\mathcal{S}, \mathcal{A}, \mathcal{P}, \mathcal{R})$ , we consider the siblings and parent nodes of the current symbolic node as the observation  $\mathcal{S}$ . The policy is defined by the distribution of tokens outputted by the RNN,  $p(\tau_i | \theta_{\text{exp}})$ , from which the action, or token  $\tau_i$ , is sampled, leading to a

transition to a new expression state. Each generation of a complete expression constitutes an episode, during which the policy RNN is guided through the computation of its reward function.

In section 3.1, we utilize the mean squared error as the loss function, optimizing constants through its minimization. Conversely, aiming for a reward function that increases in value to guide the policy more effectively, we implement squashing functions of root mean square error (RMSE) as the rewards for the sampled expression skeleton  $\tau$  in different systems:

$$\mathcal{R}_s(\tau) = \frac{1}{1 + (\sqrt{\text{MSE}_{\mathcal{F}}} + \sqrt{\text{MSE}_{\mathcal{B}}})} \quad (7)$$

$$\mathcal{R}_{s-t}(\tau) = \frac{1}{1 + (\sqrt{\text{MSE}_{\mathcal{N}}} + \sqrt{\text{MSE}_{\mathcal{B}}} + \sqrt{\text{MSE}_{\mathcal{I}}})} \quad (8)$$

**Training RNN using policy gradients** Standard policy gradient methods aim to optimize the average performance of the policy, which deviates from the objective of finding an optimal closed-form solution. To maximize the best-case performance, we employ a risk-seeking policy gradient approach introduced in Petersen et al. [22], with the learning objective  $J_{\text{risk}}(\theta_{\text{exp}}; \epsilon)$  parameterized by  $\epsilon$  as  $J_{\text{risk}}(\theta_{\text{exp}}; \epsilon) \approx \mathbb{E}_{\tau \sim p(\tau|\theta)}[\mathcal{R}(\tau) | \mathcal{R}(\tau) \geq \mathcal{R}_{\epsilon}(\theta_{\text{exp}})]$ , where  $\mathcal{R}_{\epsilon}(\theta_{\text{exp}})$  is the reward distribution’s  $(1 - \epsilon)$ -quantile under the current policy. The gradient updates generated by each batch of  $N$  sampled expressions can be articulated as Equation 9. Here,  $\tilde{\mathcal{R}}_{\epsilon}(\theta_{\text{exp}})$  represents the empirical  $(1 - \epsilon)$ -quantile of the batch rewards, while  $\mathbf{1}_x$  returns 1 if the condition is true and 0 otherwise. To foster exploration, we also integrate the entropy of the sampled expressions into the reward term, weighted by  $\lambda_{\mathcal{H}}$ [34]. Pseudo-code for SymPDE is shown in Appendix A.

$$\nabla_{\theta_{\text{exp}}} J_{\text{risk}}(\theta_{\text{exp}}; \epsilon) \approx \frac{1}{\epsilon N} \sum_{i=1}^N [\mathcal{R}(\tau^{(i)}) - \tilde{\mathcal{R}}_{\epsilon}(\theta_{\text{exp}})] \cdot \mathbf{1}_{\mathcal{R}(\tau^{(i)}) \geq \tilde{\mathcal{R}}_{\epsilon}(\theta_{\text{exp}})} \nabla_{\theta_{\text{exp}}} \log p(\tau^{(i)} | \theta_{\text{exp}}) \quad (9)$$

## 4 Experiments

We test ability of SymPDE to find closed-form symbolic solutions in the time-independent system and the spatiotemporal dynamical system respectively. For the former, we take the Poisson’s equation (equation 2) as the example, which is extensively applied across various domains such as electrodynamics, gravitation theory, and fluid dynamics. For the latter, we take the heat equation (equation 5) as the example, which plays a crucial role in delineating numerous physical processes such as heat conduction and reaction-diffusion procedures.

We compare SymPDE with a highly intuitive paradigm for discovering symbolic closed-form solutions: we self-supervisedly train PINN with sufficient epochs under the same computational domain and boundary conditions. The training points of the PINN and the outputs of the trained network serve as a new symbolic regression dataset. Using the Deep Symbolic Regression (DSR) algorithm [22], we regress the symbolic expressions of the numerical solutions as the symbolic solutions. We refer to this solution paradigm as DSR\*. Based on the expressions regressed via DSR\*, we randomly sample 100 points in the computational domain to compute the equation 7. If it satisfies the condition that the  $\mathcal{R}_s(\tau) > 0.9999$ , we regard the DSR\* algorithm as effective, capable of regressing the correct expressions of the solution; while for the symbolic solutions derived through SymPDE, we employ computer algebra systems (e.g. SymPy [30]) to rigorously ascertain whether the predicted solutions satisfy the PDEs, thereby establishing criteria for their complete recovery. The error of the numerical solutions solved by PINNs on each benchmark, as well as the benchmarks’ configurations for DSR\*, are detailed in Appendix C.

### 4.1 Time-independent system

#### 4.1.1 Solving Poisson’s equation with Nguyen benchmark suite

**Benchmark construction** To demonstrate our method’s efficacy in discerning symbolic solutions within the high-dimensional spaces of derivatives, we constructed an evaluation set based on the Nguyen benchmark suite[35] tailored to Poisson’s equation. This set encompasses twelve benchmarks,

Table 1: Average  $\mathcal{R}_s(\tau)$  and recovery rate of SympDE for 20 independent training runs on Poisson’s equation with different random seeds

Benchmark	Solution $\mathbf{u}(\mathbf{x})$	SympDE		DSR*	
		$\mathcal{R}_s(\tau)$	$P_{\text{Re}}$	$\mathcal{R}_s(\tau)$	$P_{\text{Re}}$
Nguyen-1	$x_1^3 + x_1^2 + x_1$	1.0000	100%	0.9999	100%
Nguyen-2	$x_1^4 + x_1^3 + x_1^2 + x_1$	1.0000	100%	0.9998	5%
Nguyen-3	$x_1^5 + x_1^4 + x_1^3 + x_1^2 + x_1$	1.0000	100%	0.9996	0%
Nguyen-4	$x_1^6 + x_1^5 + x_1^4 + x_1^3 + x_1^2 + x_1$	1.0000	100%	0.9959	0%
Nguyen-5	$\sin(x_1^2) \cos(x_1) - 1$	0.9376	65%	0.9998	0%
Nguyen-6	$\sin(x_1) + \sin(x_1 + x_1^2)$	1.0000	100%	0.9999	100%
Nguyen-7	$\log(x_1 + 1) + \log(x_1^2 + 1)$	1.0000	100%	0.9999	100%
Nguyen-8	$\sqrt{x_1}$	1.0000	100%	0.9999	100%
Nguyen-9	$\sin(x_1) + \sin(x_2)$	1.0000	100%	0.7461	0%
Nguyen-10	$2 \sin(x_1) \cos(x_2)$	1.0000	100%	0.8149	0%
Nguyen-11	$x_1^{x_2}$	1.0000	100%	0.9814	0%
Nguyen-12	$x_1^4 - x_1^3 + \frac{1}{2}x_2^2 - x_2$	0.7577	15%	0.4362	0%
Average		0.9746	90.0%	0.9144	33.3%

each containing: (1) A Poisson’s Equation to be solved, denoted by  $\Gamma^{(i)}, i = 1, 2, \dots, 12$ , we substitute expressions from the Nguyen benchmark as the solution function  $\mathbf{u}^{(i)}(\mathbf{x})$  into equation 2 to compute the source term  $f(\mathbf{x})$ , thus establishing the Poisson’s Equation with a corresponding closed-form solution for  $\Gamma^{(i)}$ . (2) A computational domain  $\Omega \subset \mathbb{R}^n$  where  $n$  signifies the number of independent variables in  $\Gamma^{(i)}$ . For expressions with one variable,  $\Omega$  is interval, and for expressions with two variables,  $\Omega$  is square. To ascertain the boundary conditions for  $\Gamma^{(i)}$ , we employ  $\mathbf{u}^{(i)}(\mathbf{x}), \mathbf{x} \in \partial\Omega$  as the boundary constraints. (3) A permitted set of operational symbols. The symbolic form of the source terms enables the inference of potential operators within the closed-form solution, which collectively comprise a set of permissible operators. The specific benchmarks configuration can be found in Appendix C.

**Evaluation** For each constructed benchmark, we uniformly randomly sample 100 points within the computational domain  $\Omega$  to calculate  $\text{MSE}_{\mathcal{F}}$ . For the boundary of interval, there are only two sampling points on the boundary; For the boundary of square, we uniformly randomly sample 100 points on the boundary to compute  $\text{MSE}_{\mathcal{B}}$ . To ensure the reproducibility of our experiments, we conducted twenty independent trials with different random seeds for different benchmarks. In Table 1, we report the recovery rate ( $P_{\text{Re}}$ ) of solutions and the average  $\mathcal{R}_s(\tau)$  for each benchmark. The performance of SympDE is significantly better than the DSR\* paradigm.

#### 4.1.2 Case studies: periodic potential and point charge systems

**Problem description** The Poisson’s equation is frequently employed to characterize electrostatic fields and is imbued with substantive physical significance. Considering two prevalent scenarios: equation 10 delineates the Poisson equation within a one-dimensional periodic potential field; equation 11 describes the distribution of electrostatic potential in a spherical domain  $B(0, r), r \in (0.01, 1)$ , engendered by a unit positive charge  $q$  located at the origin, essentially the fundamental solution to the Laplace equation. Note that in the vicinity of the origin, the variation of the electrostatic potential is steep. Through these instances, we aim to demonstrate the potential of SympDE in finding high-frequency or steeply varying closed-form symbolic solutions.

$$\left\{ \begin{array}{l} \frac{\partial^2 u}{\partial x^2} = -25 \sin(5x), \quad x \in [-2\pi, 2\pi] \\ u(-2\pi) = 0, \quad x = -2\pi \\ u(2\pi) = 0, \quad x = 2\pi \end{array} \right. \quad (10) \quad \left\{ \begin{array}{l} \frac{1}{r^2} \frac{\partial}{\partial r} \left( r^2 \frac{\partial u(r)}{\partial r} \right) = 0, 0.01 \leq r \leq 1 \\ u(1) = \frac{1}{4\pi}, r = 1 \\ u(0.01) = \frac{1}{0.04\pi}, r = 0.01 \end{array} \right. \quad (11)$$

**Evaluation** The comparative results of solving the same computational domain using SympDE and the DSR\* paradigm are presented in table 2. Here,  $R^2$  denotes the coefficient of determination

Table 2: Comparative Analysis of Symbolic Solutions and Their  $R^2$  Correspondence with True Solutions for Various PDE Cases via SympPDE and DSR\*

PDE	Solution	SympPDE		DSR*	
		Expression	$R^2$	Expression	$R^2$
Equation 10	$\sin(5x)$	$\sin(5x)$	1.0000	$x \cos(0.09x^2 - 3.29) - x$	0.0000
Equation 11	$\frac{1}{x^2}$	$\frac{0.07958}{x^2}$	0.9999	$0.30x^2 - 0.91x + 3.78$	0.0000
Equation 12	$x^2 e^{-t}$	$x^2 e^{-t}$	1.0000	$0.15x^2 + 0.85x^2 e^{-1.2t}$	0.9946
Equation 13	$\frac{e^{-\frac{x^2}{t}}}{\sqrt{\pi t}}$	$c_0 e^{c_1 x^2}$	0.9999	$0.79e^{-1.00\frac{x^2}{t} - 0.36t}$	0.9976

between the expressions derived from both approaches and the true solution. If  $R^2 < 0$ , we set it directly to 0. The column labeled 'expression' lists the simplified forms of the symbolic solutions found by the two paradigms. SympPDE can correctly solve both types of problems. Due to the tendency of the PINN to exhibit non-convergence in solving high-frequency problems and to fall into local optima in steep gradient problems, misleading the DSR algorithm, the correct expression could not be ascertained. The configuration for the DSR\* paradigm is provided in Appendix C, with a detailed result of the error distribution available in Appendix B.2.

## 4.2 Spatiotemporal dynamical systems

### 4.2.1 Continues time model

**Problem description** Consider a uniform thin rod of length  $l$ , with its lateral surface perfectly insulated. Given the initial temperature distribution along the rod and the temperatures at both ends of the rod, the objective is to determine the temperature distribution  $u(x, t)$  at any moment  $t > 0$ . It is known that  $u(x, t)$  satisfies a mixed problem defined by equation 12 in the region  $Q_T = [0, l] \times [0, T]$ , which specifies the initial temperature distribution  $u(x, 0)$  as well as the boundary conditions  $u(0, t)$  and  $u(l, t)$  for  $t \in [0, T]$ . Here,  $l = 1, t = 1$ .

$$\begin{cases} u_t - u_{xx} = (-x^2 - 2)e^{-t}, & (x, t) \in Q_T \\ u(x, 0) = x^2, & x \in [0, 1] \\ u(0, t) = 0, u(1, t) = e^{-t}, & t \in [0, 1] \end{cases} \quad (12)$$

**Evaluation** We randomly collect 50 points  $u(x^i, 0)$  at the initial state, 50 points  $u(0, t^i)$  and 50 sample points  $u(1, t^i)$ . Additionally, 500 points  $u(x^i, t^i)$  were uniformly randomly sampled in the  $Q_T$  region for SympPDE. We also compared SympPDE with DSR\* based on the numerical solution with a  $\mathcal{L}_2$  relative loss of 0.0283 between the numerical solution and the ground truth obtained from the trained PINN. The expressions obtained through these two distinct methodologies are depicted in table 2. It is evident that although the numerical solution of PINN is accurate enough, the deviation from the true solution is enough to mislead the DSR algorithm to find a symbolic expression that does not conform to the PDE.

### 4.2.2 Discrete time model

**Problem description** This section of the experiment addresses the problem of solving the fundamental solution to the heat equation, which can be utilized to construct classical solutions of the heat equation and holds significant physical relevance. Consider a uniform thin rod with both ends extending to infinity and its lateral surface being adiabatic. At  $t = 0$ , the temperature throughout the rod is zero, that is,  $u(x, 0) = 0$ . At this juncture, an instantaneous unit point heat source is introduced at  $x = 0$ . Consequently, for  $t > 0$ , the temperature distribution along the rod satisfies equation 13. To circumvent the challenges associated with singularities, the temperature distribution of the rod is measured at  $t = 1$  to serve as the initial condition. Subsequent measurements of the temperature at  $x = -1$  and  $x = 1$  at different moments in time are taken as boundary conditions, with the objective being to determine the temporal evolution of the temperature distribution for  $t > 0$ .



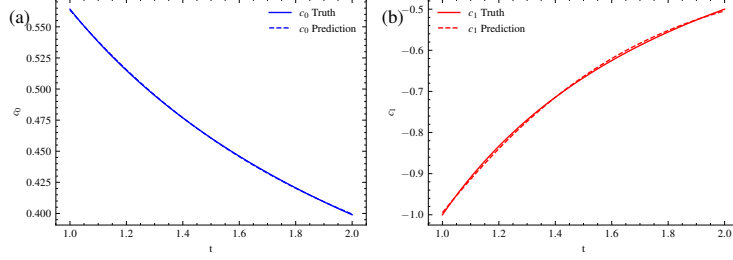


Figure 2: The parameters  $\vec{\alpha}(t; \theta_{\text{PNN}})$  of the expression skeleton of the solution to the heat equation expression skeleton found by SympPDE (a) The optimized value and the truth( $\frac{1}{\sqrt{\pi t}}$ ) of the  $c_0$  parameter (b) The optimized value and the truth( $-\frac{1}{t}$ ) of the  $c_1$  parameter

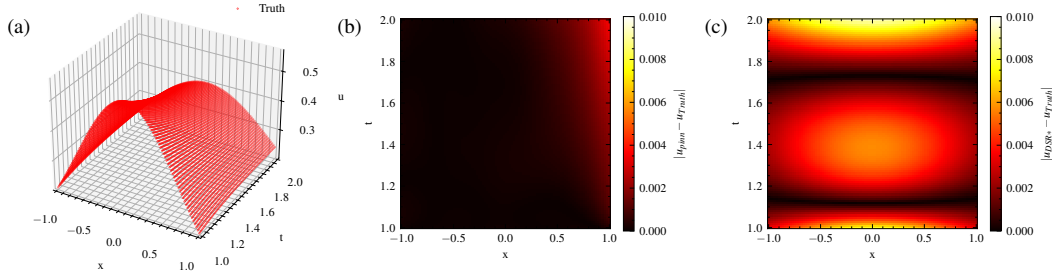


Figure 3: (a)fundamental solution of heat equation (b)Absolute error of solution via PINN (c)Absolute error of solution via DSR\*

$$\begin{cases} u_t - u_{xx} = 0, & (x, t) \in \mathbb{R} \times \mathbb{R}_+ \\ u(x, 1) = \frac{e^{-x^2}}{\sqrt{\pi}}, & x \in [-1, 1] \\ u(-1, t) = \frac{1}{\sqrt{\pi t}}, u(1, t) = \frac{e^{-\frac{1}{t}}}{\sqrt{\pi t}}, & t \in [1, 2] \end{cases} \quad (13)$$

**Evaluation** Initially, we measure (sample) the values of 100 data points at the initial condition, followed by measurements of boundary values at different moments at a frequency of 100Hz. These data are utilized to compute and guide the discovery of the correct expression skeleton. Ultimately, SympPDE find the skeleton:  $u = c_0 e^{c_1 x^2}$  as shown in table 2. We utilize the PNN to parameterize time-varying solution profiles, attaining an  $\mathcal{L}_2$  relative error between the predicted solution and the ground truth of  $9.84 \times 10^{-4}$ , in contrast to  $1.64 \times 10^{-3}$  achieved when using the PINN. The comparison of the two optimized parameters of skeleton and the true coefficient is shown in figure 2. And our solution is more interpretable than PINN. Compared with the DSR\* algorithm, we not only return the correct expression skeleton, but also get closer to the ground truth. The absolute error of DSR\* shown in figure 3, which is grossly misled, although the numerical solution of PINN has only a slight bias.

## 5 Conclusion

We introduce a deep reinforcement learning paradigm SympPDE to find the closed-form symbolic solution of various PDEs over time-independent system and spatiotemporal dynamical system. Since SympPDE is based on a deep reinforcement learning algorithm, compared to the numerical solutions of neural networks, it can find the symbolic solutions with characters of high frequency, steepness, etc., and is expected to be used to discover analytical solutions to nonlinear partial differential equations like the Navier–Stokes equations. At the same time, as a paradigm for solving symbolic solutions, SympPDE can be extensively combined with the latest end-to-end symbolic regression methods, such as X-Net proposed by Li et al. [36], to develop a more powerful method for solving symbolic solutions to PDE.

## References

- [1] Lawrence C Evans. *Partial differential equations*, volume 19. American Mathematical Society, 2022.
- [2] Dean G Duffy. *Green's functions with applications*. Chapman and Hall/CRC, 2015.
- [3] Salvatore Cuomo, Vincenzo Schiano Di Cola, Fabio Giampaolo, Gianluigi Rozza, Maziar Raissi, and Francesco Piccialli. Scientific machine learning through physics-informed neural networks: Where we are and what's next. *Journal of Scientific Computing*, 92(3):88, 2022.
- [4] Kurt Hornik, Maxwell Stinchcombe, and Halbert White. Multilayer feedforward networks are universal approximators. *Neural networks*, 2(5):359–366, 1989.
- [5] Maziar Raissi, Paris Perdikaris, and George E Karniadakis. Physics-informed neural networks: A deep learning framework for solving forward and inverse problems involving nonlinear partial differential equations. *Journal of Computational physics*, 378:686–707, 2019.
- [6] Abdul Hannan Mustajab, Hao Lyu, Zarghaam Rizvi, and Frank Wuttke. Physics-informed neural networks for high-frequency and multi-scale problems using transfer learning. *Applied Sciences*, 14(8):3204, 2024.
- [7] Lu Lu, Pengzhan Jin, Guofei Pang, Zhongqiang Zhang, and George Em Karniadakis. Learning nonlinear operators via deepnet based on the universal approximation theorem of operators. *Nature machine intelligence*, 3(3):218–229, 2021.
- [8] Zongyi Li, Daniel Zhengyu Huang, Burigede Liu, and Anima Anandkumar. Fourier neural operator with learned deformations for pdes on general geometries. *Journal of Machine Learning Research*, 24(388):1–26, 2023.
- [9] Chengping Rao, Pu Ren, Qi Wang, Oral Buyukozturk, Hao Sun, and Yang Liu. Encoding physics to learn reaction-diffusion processes. *Nature Machine Intelligence*, 5(7):765–779, 2023.
- [10] Lu Lu, Raphael Pestourie, Wenjie Yao, Zhicheng Wang, Francesc Verdugo, and Steven G Johnson. Physics-informed neural networks with hard constraints for inverse design. *SIAM Journal on Scientific Computing*, 43(6):B1105–B1132, 2021.
- [11] Ameya D Jagtap and George Em Karniadakis. Extended physics-informed neural networks (xpinn): A generalized space-time domain decomposition based deep learning framework for nonlinear partial differential equations. *Communications in Computational Physics*, 28(5), 2020.
- [12] Shengze Cai, Zhicheng Wang, Lu Lu, Tamer A Zaki, and George Em Karniadakis. Deepm&mnet: Inferring the electroconvection multiphysics fields based on operator approximation by neural networks. *Journal of Computational Physics*, 436:110296, 2021.
- [13] Zongyi Li, Nikola Kovachki, Kamyar Azizzadenesheli, Burigede Liu, Kaushik Bhattacharya, Andrew Stuart, and Anima Anandkumar. Neural operator: Graph kernel network for partial differential equations. *arXiv preprint arXiv:2003.03485*, 2020.
- [14] Zijie Li, Kazem Meidani, and Amir Barati Farimani. Transformer for partial differential equations' operator learning. *arXiv preprint arXiv:2205.13671*, 2022.
- [15] Stephanie Forrest. Genetic algorithms: principles of natural selection applied to computation. *Science*, 261(5123):872–878, 1993.
- [16] John R Koza. Genetic programming as a means for programming computers by natural selection. *Statistics and computing*, 4:87–112, 1994.
- [17] Michael Schmidt and Hod Lipson. Distilling free-form natural laws from experimental data. *science*, 324(5923):81–85, 2009.

- [18] Nicolas Staelens, Dirk Deschrijver, Ekaterina Vladislavleva, Brecht Vermeulen, Tom Dhaene, and Piet Demeester. Constructing a no-reference h. 264/avc bitstream-based video quality metric using genetic programming-based symbolic regression. *IEEE Transactions on Circuits and Systems for Video Technology*, 23(8):1322–1333, 2013.
- [19] Ignacio Arnaldo, Una-May O’Reilly, and Kalyan Veeramachaneni. Building predictive models via feature synthesis. In *Proceedings of the 2015 annual conference on genetic and evolutionary computation*, pages 983–990, 2015.
- [20] Iwo Bładek and Krzysztof Krawiec. Solving symbolic regression problems with formal constraints. In *Proceedings of the Genetic and Evolutionary Computation Conference*, pages 977–984, 2019.
- [21] Subham Sahoo, Christoph Lampert, and Georg Martius. Learning equations for extrapolation and control. In *International Conference on Machine Learning*, pages 4442–4450. Pmlr, 2018.
- [22] Brenden K. Petersen, Mikel Landajuela Larma, Terrell N. Mundhenk, Claudio Prata Santiago, Soo Kyung Kim, and Joanne Taery Kim. Deep symbolic regression: Recovering mathematical expressions from data via risk-seeking policy gradients. In *International Conference on Learning Representations*, October 2020.
- [23] Terrell Mundhenk, Mikel Landajuela, Ruben Glatt, Claudio P Santiago, Brenden K Petersen, et al. Symbolic regression via deep reinforcement learning enhanced genetic programming seeding. *Advances in Neural Information Processing Systems*, 34:24912–24923, 2021.
- [24] Wenqiang Li, Weijun Li, Lina Yu, Min Wu, Jingyi Liu, and Yanjie Li. A neural-guided dynamic symbolic network for exploring mathematical expressions from data. *arXiv preprint arXiv:2309.13705*, 2023.
- [25] Fangzheng Sun, Yang Liu, Jian-Xun Wang, and Hao Sun. Symbolic physics learner: Discovering governing equations via monte carlo tree search. *arXiv preprint arXiv:2205.13134*, 2022.
- [26] Wenqiang Li, Weijun Li, Linjun Sun, Min Wu, Lina Yu, Jingyi Liu, Yanjie Li, and Songsong Tian. Transformer-based model for symbolic regression via joint supervised learning. In *The Eleventh International Conference on Learning Representations*, 2022.
- [27] Mojtaba Valipour, Bowen You, Maysum Panju, and Ali Ghodsi. Symbolicgpt: A generative transformer model for symbolic regression. *arXiv preprint arXiv:2106.14131*, 2021.
- [28] Pierre-Alexandre Kamienny, Stéphane d’Ascoli, Guillaume Lample, and François Charton. End-to-end symbolic regression with transformers. *Advances in Neural Information Processing Systems*, 35:10269–10281, 2022.
- [29] Parshin Shojaee, Kazem Meidani, Amir Barati Farimani, and Chandan Reddy. Transformer-based planning for symbolic regression. *Advances in Neural Information Processing Systems*, 36, 2024.
- [30] Aaron Meurer, Christopher P. Smith, Mateusz Paprocki, Ondřej Čertík, Sergey B. Kirpichev, Matthew Rocklin, AmiT Kumar, Sergiu Ivanov, Jason K. Moore, Sartaj Singh, Thilina Rathnayake, Sean Vig, Brian E. Granger, Richard P. Muller, Francesco Bonazzi, Harsh Gupta, Shivam Vats, Fredrik Johansson, Fabian Pedregosa, Matthew J. Curry, Andy R. Terrel, Štěpán Roučka, Ashutosh Saboo, Isuru Fernando, Sumith Kulal, Robert Cimrman, and Anthony Scopatz. SymPy: Symbolic computing in Python. *PeerJ Computer Science*, 3:e103, January 2017. ISSN 2376-5992. doi: 10.7717/peerj-cs.103.
- [31] Lena Podina, Brydon Eastman, and Mohammad Kohandel. Universal physics-informed neural networks: symbolic differential operator discovery with sparse data. In *International Conference on Machine Learning*, pages 27948–27956. PMLR, 2023.
- [32] Ritam Majumdar, Vishal Jadhav, Anirudh Deodhar, Shirish Karande, Lovekesh Vig, and Venkataramana Runkana. Symbolic regression for pdes using pruned differentiable programs. *arXiv preprint arXiv:2303.07009*, 2023.

- [33] Dennis M Sullivan. *Electromagnetic simulation using the FDTD method*. John Wiley & Sons, 2013.
- [34] Tuomas Haarnoja, Aurick Zhou, Pieter Abbeel, and Sergey Levine. Soft actor-critic: Off-policy maximum entropy deep reinforcement learning with a stochastic actor. In *International conference on machine learning*, pages 1861–1870. PMLR, 2018.
- [35] Nguyen Quang Uy, Nguyen Xuan Hoai, Michael O’Neill, Robert I McKay, and Edgar Galván-López. Semantically-based crossover in genetic programming: application to real-valued symbolic regression. *Genetic Programming and Evolvable Machines*, 12:91–119, 2011.
- [36] Yanjie Li, Weijun Li, Lina Yu, Min Wu, Jinyi Liu, Wenqiang Li, and Meilan Hao. A novel paradigm for neural computation: X-net with learnable neurons and adaptable structure. *arXiv preprint arXiv:2401.01772*, 2024.

## A Appendix: Pseudocode for the SymPDE

---

### Algorithm 1: SymPDE for time-independent systems

---

**Data:**  $\{\mathbf{x}_f^i\}_{i=1}^{N_F}, \{\mathbf{x}_b^i, u_b^i\}_{i=1}^{N_B}$ ;

**Result:** Find a closed-form symbolic solution  $\tau : u(\mathbf{x})$  satisfying the given PDE of a time-independent system

```

1 Initialize RNN with parameters  $\theta_{exp}$ 
2 while  $\mathcal{R}_s(\tau_i) \leq 0.9999$  do
3    $\Gamma \leftarrow \{\tau_i \sim p(\tau_i|\theta_{exp})\}_{i=1}^N$  // Sample N expressions, see [22]
4    $\mathcal{L}_s \leftarrow$  automatic differentiation
5    $\Gamma \leftarrow$  Optimize Constants( $\tau_i, \mathcal{L}_s$ ) // Optimize constants
6    $\mathcal{R} \leftarrow \mathcal{R}_s(\tau_i)_{i=1}^N$  // Calculate Reward
7    $\theta'_{exp} \leftarrow \theta_{exp}$  // Update RNN by policy gradient, see [22]

```

---

### Algorithm 2: SymPDE for spatiotemporal dynamical systems

---

**Data:**  $\{\mathbf{x}_f^i\}_{i=1}^{N_N}, \{\mathbf{x}_b^i, u_b^i\}_{i=1}^{N_B}, \{\mathbf{x}_0^i, u_0^i\}_{i=1}^{N_T}$ ;

**Result:** Find a closed-form symbolic solution  $\tau : u(\mathbf{x}, t)$  satisfying the given PDE of an spatiotemporal dynamical system

```

1 Initialize RNN with parameters  $\theta_{exp}$ 
2 while  $\mathcal{R}_{s-t}(\tau_i) \leq 0.9999$  do
3    $\Gamma \leftarrow \{\tau_i \sim p(\tau_i|\theta_{exp})\}_{i=1}^N$  // Sample N expressions, see [22]
4    $\mathcal{L}_{s-t} \leftarrow$  automatic differentiation
5    $\Gamma \leftarrow$  Optimize Constants( $\tau_i, \mathcal{L}_{s-t}$ ) // Optimize constants
6    $\mathcal{R} \leftarrow \mathcal{R}_{s-t}(\tau_i)_{i=1}^N$  // Calculate Reward
7   if  $\mathcal{R}_{s-t}(\tau_i) > T$  then
8     OptimizeCoefficients( $\tau_i, \theta_{PNN}, \mathcal{L}_{s-t}$ ) // Optimize coefficients of skeletons
9     upon achieving expected reward.
9    $\theta'_{exp} \leftarrow \theta_{exp}$  // Update RNN by policy gradient, see [22]

```

---

## B Appendix: Visualized results of cases

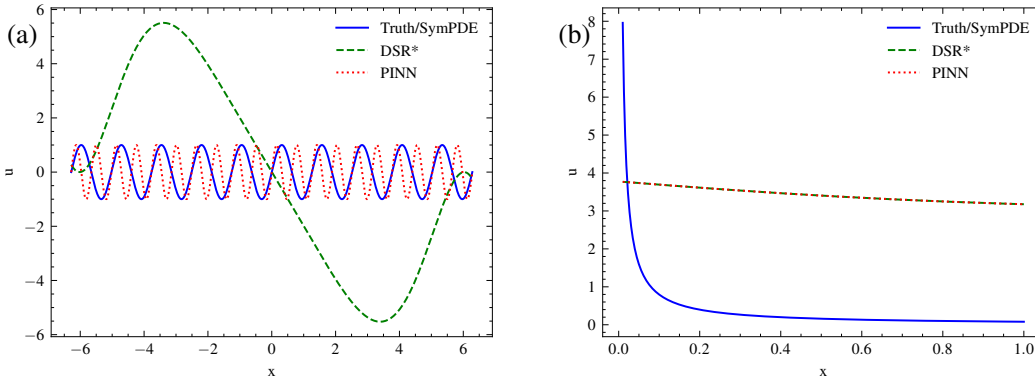


Figure B.1: (a) Results of solving equation 10 via SymPDE and DSR\* (b) Results of solving equation 11 via SymPDE and DSR\*

Figure B.1 showcases the expressions' corresponding curves for high-frequency periodic fields and point charge potential fields discovered by DSR\*. These results substantiate the inadequacies of the PINN method in fitting solutions that exhibit high-frequency oscillations and steep gradients. Specifically, PINNs demonstrate a propensity for suboptimal local convergence and an insufficiency in

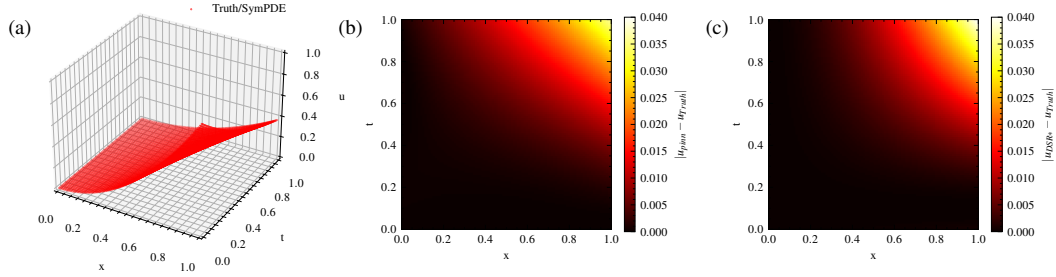


Figure B.2: (a) Truth of equation 12 (b) Absolute error of solution via PINN (b)Absolute error of solution via DSR\*

fitting capability, which are subsequently exacerbated by the symbolic regression methods, ultimately yielding expressions that are wholly unrelated to the true solutions.

Figure B.2(a) illustrates the surface of the true solution of Equation 12, where SymPDE accurately identifies the correct expression for the solution. The absolute errors between the true solution and the solutions obtained by the PINN numerical method and DSR\* are depicted respectively in figure B.2 (b)(c), further highlighting that DSR\* amplifies the numerical errors.

## C Appendix: Configurations for benchmarks and cases

Note: In the *domain* column of table C.1 C.2, *interval(a, b)* denotes a line segment with a computational domain of  $[a, b]$ , while *square(a, b)* refers to a square region with a computational domain of  $[a, b] \times [a, b]$ . Additionally, *Rectangle((a, b), (c, d))* signifies a rectangular area with a computational domain of  $[a, b] \times [c, d]$

Table C.1: Configuration of experiments on heat equation

Benchmark	SymPDE Operators	Domain	DSR* Operators
Equation 12	$\{+, -, \times, \div, \exp, x_1, x_2\}$	Square(0,1)	$\{+, -, \times, \div, \exp, x_1, x_2, \text{const.}\}$
Equation 13	$\{+, -, \times, \div, \exp, \sqrt{\bullet}, x_1, x_2\}$	Rectangle((-1,1),(1,2))	$\{+, -, \times, \div, \exp, x_1, x_2, \sqrt{\bullet}, \text{const.}\}$

Table C.2: Configuration of experiments on Poisson's equation

Benchmark	Poisson's Equation $\Delta \mathbf{u}(\mathbf{x}) = f(\mathbf{x})$	SymPDE Operators	Domain	DSR* Operators
Nguyen-1	$\mathbf{u}(\mathbf{x}) = x_1^3 + x_1^2 + x_1$ $f(\mathbf{x}) = 6x_1 + 2$	{+, -, ×, ÷, $x_1$ }	Interval(-1,1)	{+, -, ×, ÷, $x_1$ , const.}
Nguyen-2	$\mathbf{u}(\mathbf{x}) = x_1^4 + x_1^3 + x_1^2 + x_1$ $f(\mathbf{x}) = 12x_1^2 + 6x_1 + 2$	{+, -, ×, ÷, $x_1$ }	Interval(-1,1)	{+, -, ×, ÷, $x_1$ , const.}
Nguyen-3	$\mathbf{u}(\mathbf{x}) = x_1^5 + x_1^4 + x_1^3 + x_1^2 + x_1$ $f(\mathbf{x}) = 20x_1^3 + 12x_1^2 + 6x_1 + 2$	{+, -, ×, ÷, $x_1$ }	Interval(-1,1)	{+, -, ×, ÷, $x_1$ , const.}
Nguyen-4	$\mathbf{u}(\mathbf{x}) = x_1^6 + x_1^5 + x_1^4 + x_1^3 + x_1^2 + x_1$ $f(\mathbf{x}) = 30x_1^4 + 20x_1^3 + 12x_1^2 + 6x_1 + 2$	{+, -, ×, ÷, $x_1$ }	Interval(-1,1)	{+, -, ×, ÷, $x_1$ , const.}
Nguyen-5	$\mathbf{u}(\mathbf{x}) = \sin(x_1^2) \cos(x_1) - 1$ $f(\mathbf{x}) = (2 \cos(x_1) - 4x_1 \sin(x_1)) \cos(x_1^2) - (4x_1^2 + 1) \sin(x_1^2) \cos(x_1)$	{+, -, ×, ÷, sin, cos, $x_1$ }	Interval(-1,1)	{+, -, ×, ÷, sin, cos, $x_1$ , const.}
Nguyen-6	$\mathbf{u}(\mathbf{x}) = \sin(x_1) + \sin(x_1 + x_1^2)$ $f(\mathbf{x}) = -(2x_1 + 1)^2 \sin(x_1^2 + x_1) - \sin(x_1) + 2 \cos(x_1^2 + x_1)$	{+, -, ×, ÷, sin, cos, $x_1$ }	Interval(-1,1)	{+, -, ×, ÷, sin, cos, $x_1$ , const.}
Nguyen-7	$\mathbf{u}(\mathbf{x}) = \log(x_1 + 1) + \log(x_1^2 + 1)$ $f(\mathbf{x}) = -4x_1^2 / (x_1^2 + 1)^2 + 2 / (x_1^2 + 1) - 1 / (x_1 + 1)^2$	{+, -, ×, ÷, log, $x_1$ }	Interval(-1,1)	{+, -, ×, ÷, log, $x_1$ , const.}
Nguyen-8	$\mathbf{u}(\mathbf{x}) = \sqrt{x_1}$ $f(\mathbf{x}) = -0.25 / x_1^{1.5}$	{+, -, ×, ÷, log, exp, $x_1, x_2$ }	Square(0.5,1.5)	{+, -, ×, ÷, log, exp, $x_1, x_2$ , const.}
Nguyen-9	$\mathbf{u}(\mathbf{x}) = \sin(x_1) + \sin(x_2^2)$ $f(\mathbf{x}) = 2 \cos(x_2^2) - 4x_2^2 \sin(x_2^2) - \sin(x_1)$	{+, -, ×, ÷, sin, cos, $x_1, x_2$ }	Square(0.5,1.5)	{+, -, ×, ÷, sin, cos, $x_1, x_2$ , const.}
Nguyen-10	$\mathbf{u}(\mathbf{x}) = 2 \sin(x_1) \cos(x_2)$ $f(\mathbf{x}) = -4 \sin(x_1) \cos(x_2)$	{+, -, ×, ÷, sin, cos, $x_1, x_2$ }	Square(0.5,1.5)	{+, -, ×, ÷, sin, cos, $x_1, x_2$ , const.}
Nguyen-11	$\mathbf{u}(\mathbf{x}) = x_1^{x_2}$ $f(\mathbf{x}) = x_1^{x_2} \log(x_1)^2 + x_1^{x_2} x_2 (x_2 - 1) / x_1^2$	{+, -, ×, ÷, log, exp, $x_1, x_2$ }	Square(0.5,1.5)	{+, -, ×, ÷, log, exp, $x_1, x_2$ , const.}
Nguyen-12	$\mathbf{u}(\mathbf{x}) = x_1^4 - x_1^3 + \frac{1}{2} x_2^2 - x_2$ $f(\mathbf{x}) = 12x_1^2 - 6x_1 + 1.0$	{+, -, ×, ÷, $x_1, x_2$ }	Square(0.5,1.5)	{+, -, ×, ÷, $x_1, x_2$ , const.}
Equation 10	$\mathbf{u}(\mathbf{x}) = \sin(5x_1)$ $f(\mathbf{x}) = -25 \sin(25x_1^2)$	{+, -, ×, ÷, sin, cos, $x_1$ }	Interval(-2 $\pi$ , 2 $\pi$ )	{+, -, ×, ÷, sin, cos, $x_1$ , const.}
Equation 11	$\mathbf{u}(\mathbf{x}) = \frac{1}{4\pi x_1}$ $f(\mathbf{x}) = 0$	{+, -, ×, ÷, $x_1$ , const.}	Interval(0.01,1.00)	{+, -, ×, ÷, $x_1$ , const.}